Cardiovascular Engineering and Technology, Vol. 10, No. 3, September 2019 *(© 2019)* pp. 531–542
https://doi.org/10.1007/s13239-019-00426-1

Original Article

Design and Computational Validation of a Novel Bioreactor for Conditioning Vascular Tissue to Time-Varying Multidirectional Fluid Shear Stress

Janet Liu, Kurtis Cornelius, Mathew Graham, Tremayne Leonard, Austin Tipton, Abram Yorde, and Philippe Sucosky

Department of Mechanical and Materials Engineering, Wright State University, 257 Russ Engineering Center, Dayton, OH 45435, USA

(Received 18 February 2019; accepted 4 July 2019; published online 15 July 2019)

Associate Editor Ajit P. Yoganathan and Hanjoong Jo oversaw the review of this article.

Abstract
Purpose—The cardiovascular endothelium experiences pulsatile and multidirectional fluid wall shear stress (WSS). While the effects of non-physiologic WSS magnitude and pulsatility on cardiovascular function have been studied extensively, the impact of directional abnormalities remains unknown due to the challenge to replicate this characteristic in vitro. To address this gap, this study aimed at designing a bioreactor capable of subjecting cardiovascular tissue to time-varying WSS magnitude and directionality.
Methods—The device consisted of a modified cone-and-plate bioreactor. The cone rotation generates a fluid flow subjecting tissue to desired WSS magnitude, while WSS directionality is achieved by altering the alignment of the tissue relative to the flow at each instant of time. Computational fluid dynamics was used to verify the device ability to replicate the native WSS of the proximal aorta. Cone and tissue mount velocities were determined using an iterative optimization procedure.
Results—Using conditions derived from cone-and-plate theory, the initial simulations yielded root-mean-square errors of 22.8 and 8.4% in WSS magnitude and angle, respectively, between the predicted and the target signals over one cycle, relative to the time-averaged target values. The conditions obtained after two optimization iterations reduced those errors to 3.5 and 0.5%, respectively, and generated 0.2% and 0.01% difference in time-averaged WSS magnitude and angle, respectively, relative to the target waveforms.
Conclusions—A bioreactor capable of generating simultaneously desired time-varying WSS magnitude and directionality was designed and validated computationally. The ability to subject tissue to *in vivo*-like WSS will provide new insights into cardiovascular mechanobiology and disease.

Keywords—Cardiovascular, Fluid wall shear stress, Mechanobiology, Hemodynamics, Directionality.

Address correspondence to Philippe Sucosky, Department of Mechanical and Materials Engineering, Wright State University, 257 Russ Engineering Center, Dayton, OH 45435, USA. Electronic mail: liu.77@wright.edu, cornelius.15@wright.edu, graham.181@wright.edu, leonard.84@wright.edu, tipton.54@wright.edu, yorde.3@wright.edu, philippe.sucosky@wright.edu

INTRODUCTION

Cardiovascular structures interact with their surrounding mechanical environment to drive critical cell-extracellular matrix processes. In particular, local hemodynamic factors, such as the fluid wall shear stress (WSS) induced by blood flow, are known to alter the expression of endothelial and smooth muscle cell phenotypes.[29,30,35] The ability of WSS to maintain tissue homeostasis by increasing endothelial cell migration, permeability, proliferation and activating certain transcription factors has been documented in numerous studies.[13,18,29,31] Conversely, WSS abnormalities tend to trigger biological cascades leading to disease.[11]

A major challenge in the isolation of the cause-and-effect relationships between cardiovascular biology and hemodynamics is the difficulty to replicate *in vitro* the full spectrum of the native flow characteristics, which include three-dimensionality, pulsatility and multidirectionality.[10] Parallel plate devices have been used in early mechanobiological studies aimed at investigating the effects of WSS magnitude or directionality on the vascular endothelium. Those devices consist of a pump driving a flow of culture medium between two plates, exposing in turn the cells seeded

along the bottom plate to unidirectional WSS. Parallel plate systems are typically limited to the production of steady uniform WSS due to the inertia of their driving components and of the large volume of working fluid. However, in a recent design variation, the implementation of a rotating glass slide seeded with cells enabled discrete changes in flow direction.[48] The device was used to evidence the switch of the endothelial response from atheroprotective to atheroprone when the flow orientation was changed from 180° to 90°.[47] Orbital shakers have also been used to subject cells grown in Petri dishes to biaxial oscillatory WSS, and have demonstrated the preferential cell alignment with the direction of the largest WSS component and a more random orientation under low-magnitude biaxial WSS.[12]

Previous investigations of the biological response of endothelial cells to WSS have also implemented cone-and-plate bioreactors. These devices, which are derived from cone-and-plate viscometers, consist of an inverted cone rotating above a stationary plate supporting the cells.[34] The rotation of the cone generates a flow of culture medium above the plate, resulting in turn in the generation of WSS on the cell monolayer. Under certain conditions (low Reynolds number, small cone-plate angle α, no gap between the cone apex and the plate), the device generates a uniform circumferential WSS on the plate,[6,14,20,37,38] making it a convenient tool for the production of a well-controlled, time-varying WSS environment. In its practical implementation, however, the finite gap h between the cone apex and the plate makes the WSS become spatially dependent, with a local magnitude τ at any radial location r proportional to the cone velocity ω, and the fluid dynamic viscosity μ,[40]

$$\tau = \mu\omega \frac{r}{h + r\alpha}. \quad (1)$$

Such devices have been used to study the response of vascular endothelial cells to physiologic and atherosclerotic WSS,[15,17] and WSS signaling in the valvular endothelium.[19] The need to elucidate the role of cell-extracellular matrix communication in WSS signaling has motivated the design of more sophisticated cone-and-plate devices capable of subjecting whole pieces of cardiovascular tissue to WSS.[40,42] In their typical implementation, tissue specimens are sutured on the plate and conditioned to WSS for 48 to 72 h. The specimens are then harvested and either mounted in OCT compound for immunohistochemistry analyses, or flash frozen with liquid nitrogen for western blotting or zymography. The use of whole pieces of tissue as opposed to cells enables the quantification of protein expression and enzymatic activity. The comparison of the biological results obtained on fresh specimens and specimens subjected to physiologic and pathologic WSS allows for the assessment of the impact of a particular WSS environment on the tissue biological signature. Such devices have been successfully implemented to evidence the key role played by WSS abnormalities in calcific aortic valve disease and bicuspid aortic valve aortopathy.[1,3,23,39,41,43,44]

Despite these advances, cone-and-plate bioreactors remain limited to the generation of a uniaxial circumferential WSS, which is a crude approximation of the multidirectional WSS environment typically observed in the vasculature.[10,28,36,46] While orbital shakers can subject cells to continuous changes in WSS directionality, they do not provide simultaneous control over WSS direction and magnitude. Lastly, the parallel-plate device featuring a rotating glass slide improves on the level of control over WSS magnitude but is limited to discrete changes in flow orientation. Flow characterizations in aortas,[24,27] aortic valves,[5,7–9,33] cerebral aneurysms,[21,25,26,49] and atherosclerotic blood vessels[22,45] have evidenced increased helicity and WSS multidirectionality, which may promote disease development.[2,16] The availability of a device capable of recapitulating the temporal variations in WSS magnitude and directionality observed *in vivo* would advance the elucidation of cardiovascular disease. Therefore, the objective of this study was to design a novel bioreactor capable of subjecting cardiovascular tissue specimens to controlled time-varying WSS magnitude and directionality. The demonstrated ability of the cone-and-plate bioreactor to generate large temporal gradients in WSS magnitude, such as those typically experienced by the vascular endothelium, motivates its use for the replication of native WSS waveforms. This paper describes a design solution based on the cone-and-plate principle and featuring an innovative rotating tissue mount system to provide dynamic and continuous control over WSS directionality. Operating conditions generating a physiologically relevant WSS environment were determined using computational fluid dynamics (CFD) simulations.

MATERIALS AND METHODS

Design Solution

Overview

The bioreactor was based on the cone-and-plate system previously designed in our laboratory to subject cardiovascular tissue to time-varying WSS.[40] Given the capability of this device to generate WSS exclusively along the circumferential direction, changes in WSS directionality were achieved by altering the orientation

of the tissue specimens relative to the flow direction. The original design was therefore adapted to implement rotating tissue mounts. The new system consists of a cone assembly, a tissue mount assembly, and a perfusion system (Fig. 1).

Cone Assembly: Generation of WSS Magnitude

The function of the cone assembly is to generate desired temporal variations in WSS magnitude. Consistent with our previous design, this assembly consists of a Delrin cone (radius: 80 mm; angle: 179°) attached to an aluminum shaft, which is coupled to the servo motor via a helical coupling (61005K191, McMaster-Carr, Aurora, OH). These components are located within the culture chamber, above the circular plate and the tissue samples (Fig. 2a). The plate is mounted 200 μm below the cone apex, on top of a stainless-steel collector chamber, and features four equi-angularly spaced holes (diameter: 8 mm, radial location: 20 mm from the plate center) exposing the tissue samples to flow. The collector chamber, the lid and the plate form an enclosed space filled with culture medium (Dulbecco's Modified Eagle's Medium-high glucose, Sigma-Aldrich Co., St. Louis, MO).

Tissue Mount Assembly: Generation of WSS Directionality

The tissue mount assembly is the key component that distinguishes this new cone-and-plate bioreactor from our previous design.[40] The function of the tissue mount assembly is to generate temporal changes in the relative alignment between the tissue samples and the circumferential flow. The tissue mount assembly consists of four stainless-steel mounts driven by a main aluminum driving shaft (diameter: 3.2 mm; length: 28.0 mm) and a 14-tooth gear (57655K33, McMaster-Carr) via a flexible coupling (6208K425, McMaster-Carr) (Fig. 2a). Each mount consists of a circular platform (diameter: 7 mm) featuring eight peripheral pinholes to suture the tissue (Fig. 2b). The size of the platform was selected to accommodate a tissue specimen sufficiently large to yield enough protein content for subsequent biological analyses, but sufficiently small so that the WSS signal generated by the bioreactor effectively represents the local WSS experienced *in vivo* by this circular tissue region. The platform is connected to a top driving shaft (section 1 diameter: 4.8 mm; section 1 length: 14.0 mm; section 2 diameter: 3.2 mm; section 2 length: 11.0 mm). The vertical position of each mount can be adjusted by sliding and fastening the tissue mount in the helical coupling to ensure that the tissue top surface is leveled with the circular plate. Practically, following the suturing of the tissue specimens to the tissue mounting platforms (Fig. 3a), a cylindrical insert will be placed above the plate (Fig. 3b), and each tissue mount will be adjusted vertically via the helical coupling until the top tissue surface is in contact with the insert (Fig. 3c). Lastly the helical coupling will be tightened to maintain the tissue mount in position (Fig. 3d). After repeating this procedure with all specimens, the insert will be removed from the plate (Fig. 3e). The tissue mounting platform and the plate holes were designed to allow for a 500-μm radial gap between the edge of the tissue specimens and the edge of the plate holes (see Fig. 3d), to prevent friction between the rotating tissue and the stationary plate, and to allow for a small misalignment between

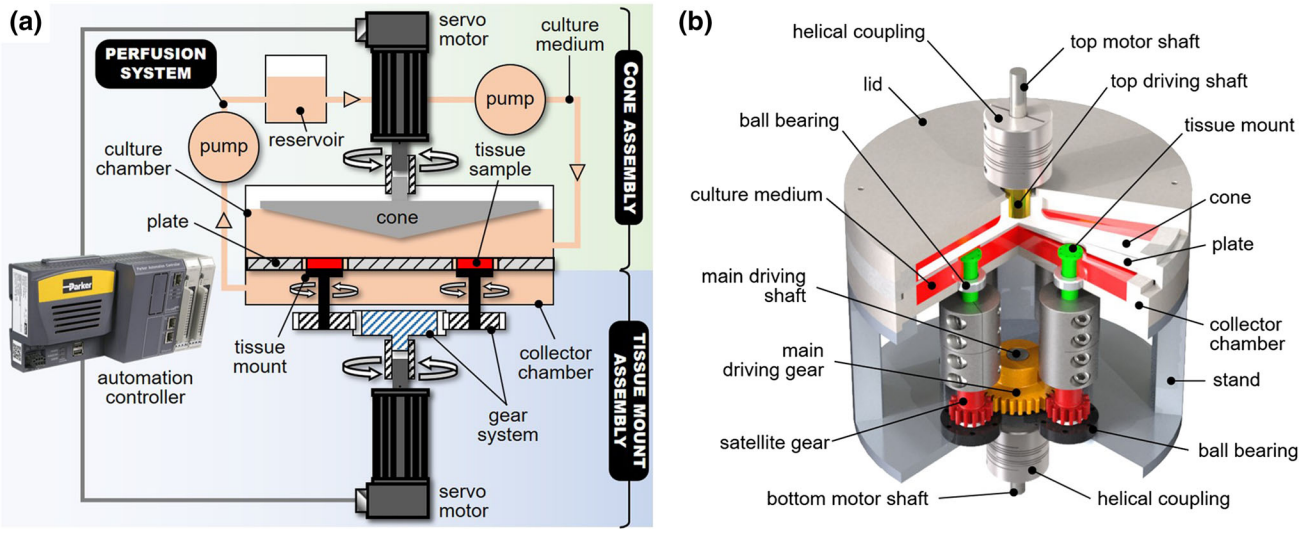

FIGURE 1. Multidirectional WSS bioreactor design: (a) schematic showing the cone assembly, tissue mount assembly, and perfusion system; and (b) assembled bioreactor system components.

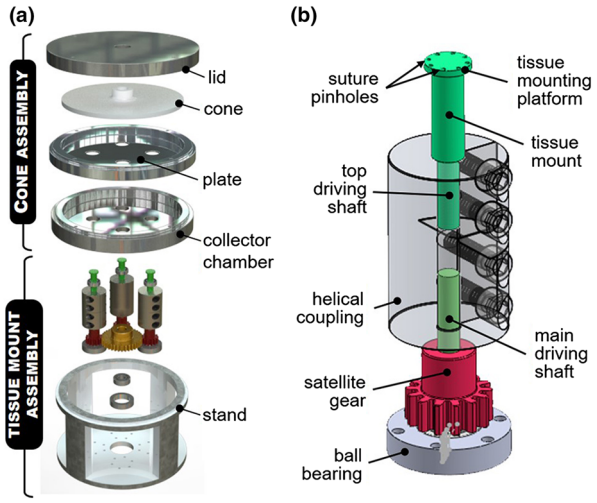

FIGURE 2. Design solution description: (a) exploded view; and (b) tissue mount components.

the axis of the tissue mount and the axis of the circular hole machined in the plate.

The tissue mount assembly is housed in an aluminum cylindrical support, and is driven by a second servo motor via a 16-tooth gear (57655K34, McMaster-Carr) and a helical coupling (61005K191, McMaster-Carr). Four tissue mounts are equi-angularly placed on the plate to minimize the impact of downstream flow disturbances caused by each sample, while enabling the conditioning of a sufficient amount of tissue for subsequent biological analyses. A programmable automation controller (PAC320, Parker-Hannifin) is used to interface between the two servo motors and to ensure the synchronous rotation of the cone and the mounts.

Perfusion System

Two peristaltic pumps (SP200, APT Instruments, Rochester, IL) are used to circulate culture medium through the system. One pump drives fresh culture medium from an external stainless-steel reservoir (volume: 175 mL) into the bioreactor, while the other returns culture medium from the collector chamber to the reservoir. The pump flow rate (0.92 mL/min) was chosen to enable full replenishment of the bioreactor every hour.

Computational Fluid Dynamics (CFD) Modeling

Although the ability of the cone assembly to provide control over the magnitude of the circumferential WSS through Eq. (1) has been demonstrated previously,[40,42] the rotation of the tissue in this new design was expected to generate flow perturbations, affecting the validity of this equation. Therefore, an iterative CFD strategy was implemented to determine appropriate operating conditions (i.e., cone and tissue rotation waveforms) enabling the replication of a target WSS environment.

Geometry and Boundary Conditions

Given the angular symmetry of the device, a 90° slice of the bioreactor was modeled in SolidWorks (Dassault Systèmes SolidWorks Corporation, Waltham, MA) and imported in ANSYS CFX (Ansys, Inc, Canonsburg, PA). The geometry consisted of the fluid domain (i.e., culture medium) located within the culture chamber and bounded by the cone surface, the plate, and the top surface of the tissue samples (Fig. 4). To simplify the geometry, the 500-μm radial gap between each sample and the plate was discarded. This idealization is not expected to affect substantially the WSS environment for two reasons: (1) it is very small relative to the diameter of the tissue specimens (7 mm) and the radius of the plate (40 mm); and (2) the WSS on the tissue surface is mostly dependent on the spatial velocity gradient generated above the tissue surface. The cone and tissue surfaces were treated as rotating walls with a no-slip condition, while the plate was

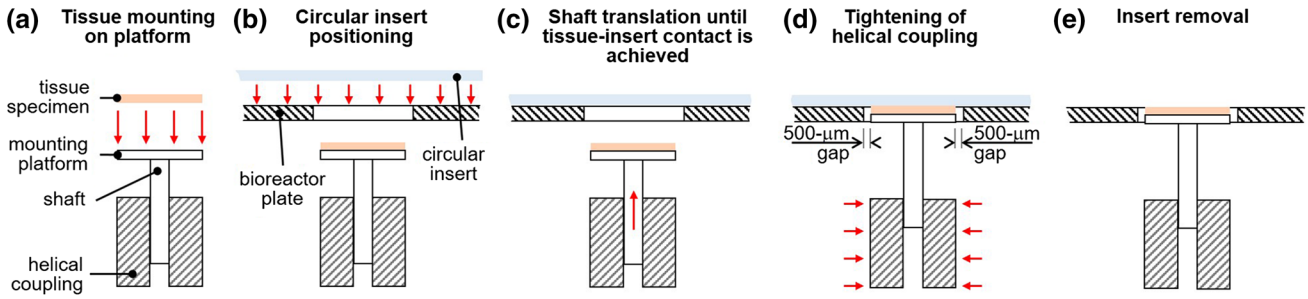

FIGURE 3. Schematic of the procedure for tissue flush-mounting with the plate: (a) the tissue specimen is sutured to the mounting platform; (b) a circular insert is placed on top of the plate; (c) the tissue mounting platform is raised until the tissue makes contact with the insert; (d) the helical coupling is tightened; and (e) the insert is removed from the plate.

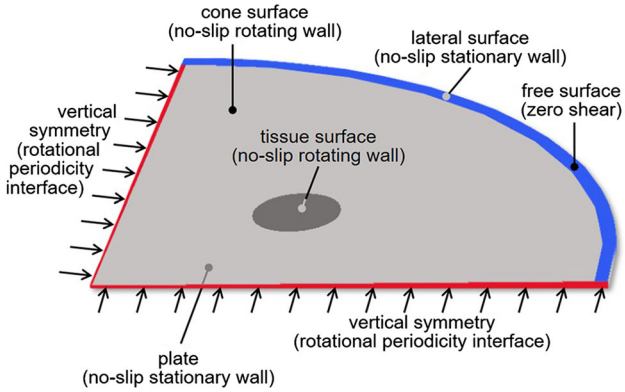

FIGURE 4. Bioreactor computational domain and boundary conditions.

defined as a stationary no-slip surface. The free-surface of the fluid domain (i.e., culture medium surface in contact with the air gap within the lid) was treated as a zero-shear surface. A rotational periodicity condition was imposed on the two vertical symmetry sections of the geometry. The culture medium (Dubelcco's Modified Eagle's Medium—high glucose, Sigma-Aldrich, St Louis, MO) was modeled as a Newtonian fluid with a density of 1040 ± 9 kg/m^3 and a kinematic viscosity of 0.95 ± 0.01 cSt, as determined experimentally over 5 measurements at 37°C (i.e., incubator temperature) using a scale and a U-tube viscometer, respectively.

Mesh Sensitivity Analysis

A mesh sensitivity analysis was performed to determine the appropriate mesh characteristics generating grid-independent flow results. The three-dimensional domain was meshed using tetrahedral elements. Different computational grids were investigated by increasing the number of elements across the gap between the cone apex and the plate from 3 to 7, which resulted in grid sizes between 1.2 and 15 million elements. For those simulations, the test case consisted of a steady cone rotation of 98.6 rad/s (with no tissue rotation) to generate a target WSS of 5 Pa on the tissue surface (as prescribed by Eq. (1)). The flow velocity was captured at a point located 100 μm above the center of the tissue surface. Mesh independence was considered to be achieved when a mesh generated less than 2% change in flow velocity relative to the immediately coarser mesh.

Determination and Validation of Device Operating Conditions

The impact of tissue rotation on the magnitude of the WSS generated on the tissue surface was compensated for by following an iterative optimization method. To demonstrate the applicability of this procedure to the generation of physiologically relevant WSS environments, the method was implemented to determine the operating conditions enabling the replication

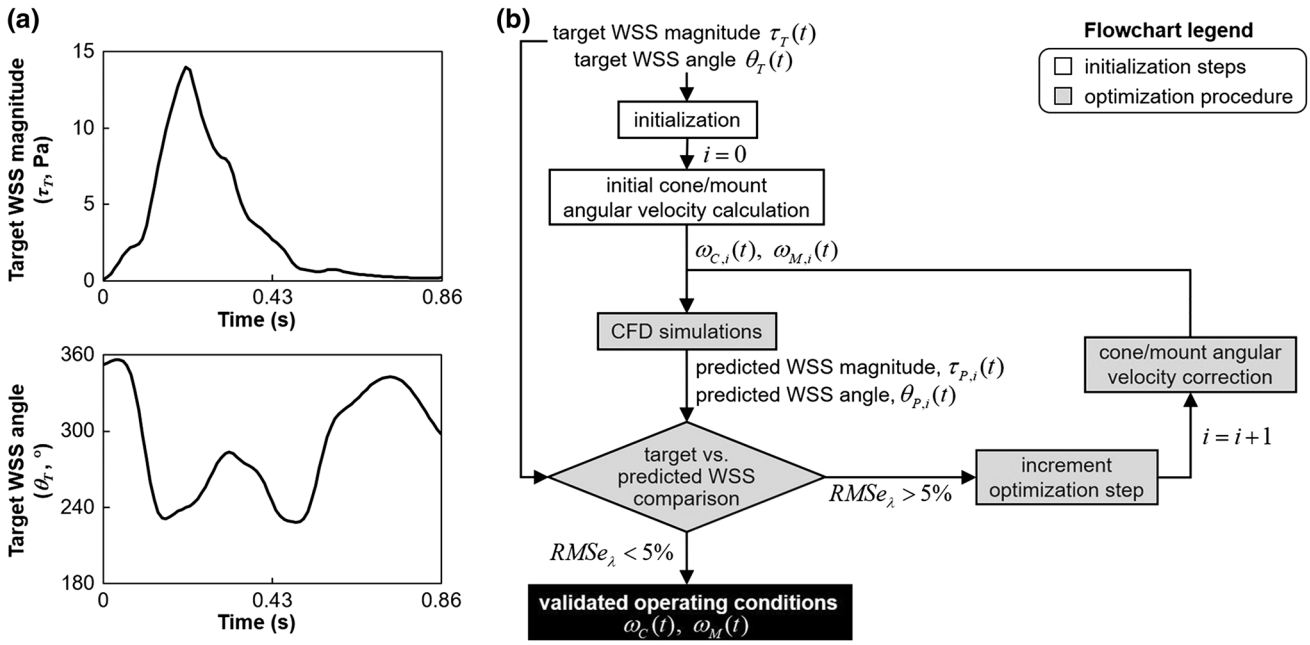

FIGURE 5. Determination of operating conditions: (a) target WSS magnitude and angle characteristics (angular values represent the angle between the instantaneous WSS vector and the longitudinal streamwise direction on the aortic wall convexity); and (b) iterative optimization flowchart.

of the native WSS on the convexity of the proximal ascending aorta. The temporal characteristics of the WSS vector at that specific location were obtained from the literature[7,32] and were defined by a magnitude varying between 0 and 13.8 Pa, and an angular span of 123° during one cardiac cycle (Fig. 5a).

The iterative optimization procedure consisted of four steps (Fig. 5b). First, the target temporal variations in WSS angle (θ_T) were converted into a mount angular velocity waveform ($\omega_{M,0}$) via the following equation:

$$\omega_{M,0} = \frac{d\theta_T}{dt} \tag{2}$$

The target temporal variations in WSS magnitude (τ_T) were converted into a cone angular velocity waveform ($\omega_{C,0}$) using Eq. (1). Following the prescription of both angular velocity waveforms as boundary conditions in the CFD model, flow simulations were performed over two cycles to eliminate initial transient effects, and the predicted WSS characteristics on the tissue surface were extracted over the second cycle using a time step of 2.5 ms.

Comparisons between the predicted and target WSS characteristics (i.e., magnitude and angle) were quantified in terms of the normalized root-mean-square error over one cycle RMSe_λ defined as

$$\mathrm{RMSe}_\lambda = \frac{\sqrt{\frac{1}{N}\sum_{i=1}^{N}\left(\lambda_{P,i} - \lambda_{T,i}\right)^2}}{\frac{1}{N}\sum_{i=1}^{N}\lambda_{T,i}}, \tag{3}$$

where λ represents WSS magnitude (τ) or angle (θ), the subscripts $_T$ and $_P$ define target and predicted values, respectively, and N is the number of time steps in one period. Validation of the cone and tissue mount angular velocity waveforms required the following criterion to be satisfied:

$$\mathrm{RMSe}_\lambda < 5\% \tag{4}$$

Should this criterion not be satisfied, the optimization procedure was initiated. At each iteration i of this procedure, a corrected cone velocity $\omega_{C,i}$ was calculated via implementation of a scaling factor,

$$\omega_{C,i} = \frac{\tau_{P,i-1}}{\tau_T}\omega_{C,i-1} \tag{5}$$

Similarly, a corrected tissue mount angular velocity $\omega_{M,i}$ was calculated as

$$\omega_{M,i} = \omega_{M,i-1} + \frac{d}{dt}\left(\theta_T - \theta_{P,i-1}\right) \tag{6}$$

The corrected waveforms were input to the CFD model and new simulations were performed. This optimization process was implemented iteratively until the validation criterion described in Eq. (4) was met.

Torque Requirements and Servo Motor Selection

The servo motors driving the cone and the tissue mount systems were selected based on torque requirements, which were determined following the completion of the optimization procedure. The torque needed to rotate the cone assembly (T_C) and tissue mount assembly (T_M) must balance the resisting torque imposed by the fluid and the acceleration torque of the cone/tissue mounts, and are therefore calculated as

$$T_C = T_{\mathrm{fluid},C} + I_C\frac{d\omega_C}{dt}, \tag{7}$$

and

$$T_M = 4T_{\mathrm{fluid,M}} + \left(4I_M + I_{\mathrm{MDS}}\frac{N_M}{N_{\mathrm{MDS}}}\right)\frac{d\omega_M}{dt}, \tag{8}$$

respectively, where $T_{\mathrm{fluid,C}}$ and $T_{\mathrm{fluid,M}}$ are the viscous torques imposed by the fluid on the cone and a tissue mount, respectively, I_C, I_M and I_{MDS} are the moment of inertia of the cone assembly (i.e., cone and shaft), the tissue mount assembly (i.e., one tissue mount attached to its cylindrical shaft) and the main tissue mount driving shaft, respectively, and N_M and N_{MDS} are the numbers of teeth on the tissue mount and main driving shaft gears, respectively ($N_M = 14$, $N_{\mathrm{MDS}} = 16$). The moment of inertia for the cone assembly I_C was calculated as

$$I_C = \frac{3}{10}m_C R_C^2 + \frac{1}{2}m_{\mathrm{TDS}}R_{\mathrm{TDS}}^2, \tag{9}$$

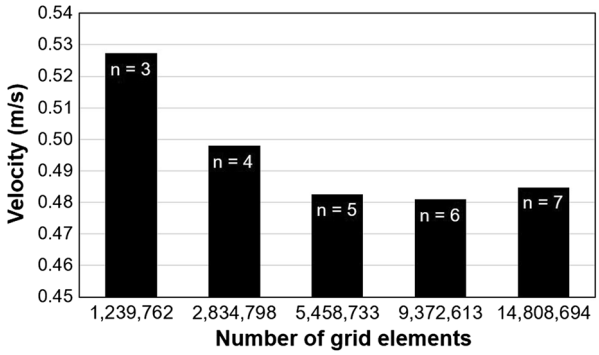

FIGURE 6. Mesh sensitivity results: velocity predictions at a point located 100 μm above the center of the tissue surface as a function of number of grid elements (n: number of elements in the gap between the cone apex and the plate).

TABLE 1. Variations of the normalized RMS error during the iterative optimization procedure.

Optimization step	WSS magnitude normalized RMS error, $RMSe_\tau$ (%)	WSS angle normalized RMS error, $RMSe_\theta$ (%)
Initial simulation (pre-optimization)	22.7	8.5
1st optimization iteration	3.5	8.3
2nd optimization iteration	3.5	0.5

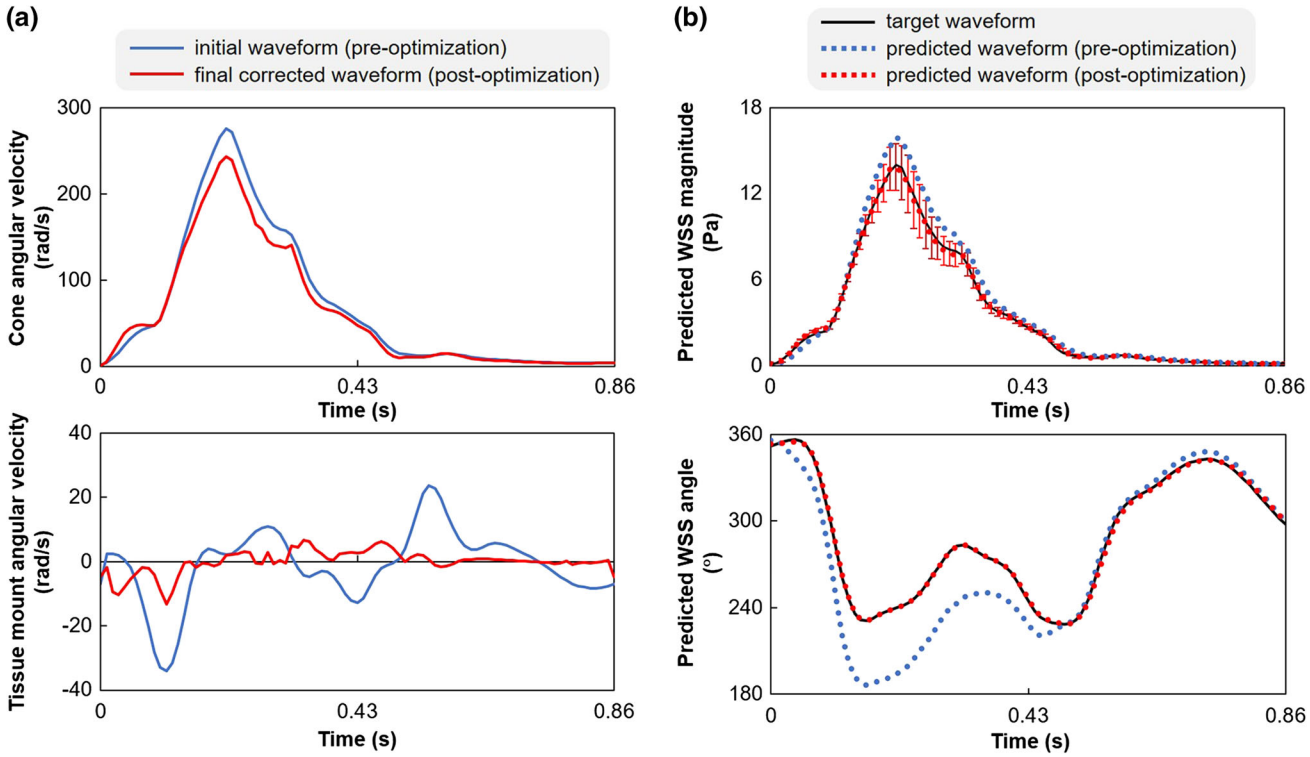

FIGURE 7. Pre- and post-optimization operating conditions and WSS characteristics: (a) cone and tissue mount angular velocities; and (b) WSS magnitude and angle predictions on tissue surface (error bar: WSS standard deviation).

where m_C and m_{TDS} are the mass, and R_C and R_{TDS} are the radii of the cone and the top driving shaft, respectively. Similarly, the moment of inertia for the tissue mount I_M was calculated as

$$I_M = \frac{1}{2} m_M R_M^2, \tag{10}$$

where m_M and R_M are the mass and radius of one tissue mount, respectively. Lastly, the moment of inertia of the tissue mount main driving shaft was calculated as

$$I_{MDS} = \frac{1}{2} m_{MDS} R_{MDS}^2, \tag{11}$$

where m_{MDS} and R_{MDS} are the mass and radius of the shaft.

RESULTS

Mesh Characteristics

The results of the mesh sensitivity analysis are reported in Fig. 6. An increase in the minimum number of elements from 4 to 5 in the gap between the cone and the plate resulted in a 193% increase in the number of cells in the computational grid, and a 3.1% change in predicted velocity 100 μm above the center of the tissue surface. The addition of one more element (n = 6) increased the total number of cells by 172% and resulted in a 0.3% change in predicted velocity, which met the criterion for mesh independence. This meshing strategy resulted in a computational grid of 9.3 million elements.

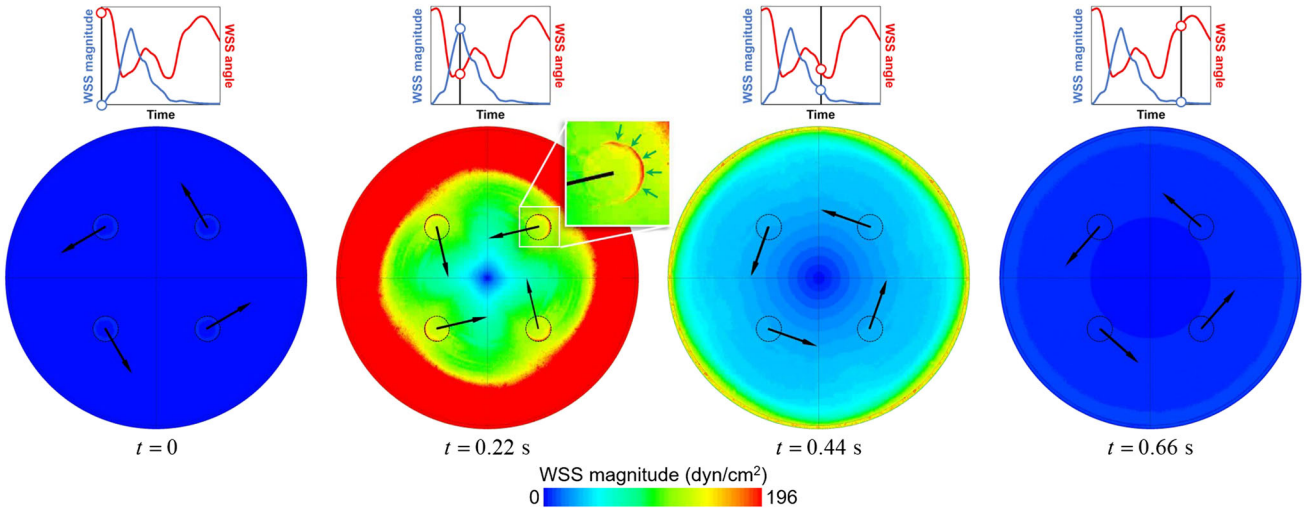

FIGURE 8. Time history of post-optimization WSS spatial distribution on bioreactor plate and tissue surface (black circle: outline of tissue circumference; black arrow: WSS vector direction; inset: magnified view of WSS distribution on tissue surface; green arrows: high WSS concentrations).

TABLE 2. Predicted torque characteristics for cone and tissue mount assemblies.

Characteristics	Cone assembly	Tissue mount assembly
RMS torque (N m)	7.8×10^{-2}	1.7×10^{-5}
Peak torque (N m)	1.9×10^{-1}	3.9×10^{-5}
Average velocity (rpm)	583	20
Maximum velocity (rpm)	2324	111

CFD Analysis

Operating Conditions and Optimization Results

Following the initial simulation implementing cone and tissue mount angular velocities directly derived from Eqs. (1) and (2), two optimization iterations were needed to satisfy the WSS magnitude and angle validation criteria ($RMSe_\tau = 3.5\%$ and $RMSe_\theta = 0.5\%$; Table 1). The operating conditions resulting from the optimization procedure consisted of a cone angular velocity varying between 0.9 and 243.3 rad/s (time average: 61.1 rad/s, standard deviation: 71.1 rad/s), and a tissue mount angular velocity varying between − 13.3 and 6.6 rad/s (time average: 4.1 rad/s, standard deviation: 3.6 rad/s; Fig. 7a). Therefore, while the corrected cone velocity was qualitatively similar to the initial waveform (only 10% change in time-average angular velocity), the correction applied to the tissue mount velocity was more substantial (85% change in time-average angular velocity). These optimized operating conditions generated a WSS environment on the tissue surface that closely mimicked the magnitude and angular characteristics of the target WSS signal (0.2% difference in time-averaged WSS magnitude, 0.01% difference in time-averaged WSS angle; Fig. 7b).

WSS Spatial Distribution and Design Justifications

Following this optimization procedure, the WSS environment on the tissue surface was further characterized in terms of its spatial distribution. At each instant of time and consistent with Eq. (1), the WSS environment generated on the plate exhibited spatial variations along the radial direction (Fig. 8). At time points corresponding to elevated WSS, this radial distribution is disturbed by the no-slip condition imposed on the rotating tissue, resulting in a local concentration of WSS near the edge of the tissue specimen (see inset at $t = 0.22$ s). Importantly, the local disturbances generated downstream from a specimen vanish over a short distance and never reach the next specimen, which justifies the angular spacing between specimens. Quantitatively, the bioreactor subjected the tissue surface to moderate WSS spatial variations as suggested by the relatively low WSS standard deviations captured on the tissue surface throughout the cycle (cycle-averaged standard deviation: 9.2% of surface-averaged WSS; peak standard deviation: 15.8% of surface-averaged WSS at $t = 0.22$ s; see error bars in Figure 7b). Overall, those results suggest the existence of a relatively uniform WSS environment on the tissue surface, and the absence of fluid dynamic

interactions between one specimen and the one downstream.

Torque Results and Servo Motor Selection

The calculation of the moment of inertia for the different rotating components of the design yielded $I_C = 8.5 \times 10^{-5}$ kg m^2, $I_M = 8.5 \times 10^{-9}$ kg m^2, and $I_{MDS} = 8.2 \times 10^{-9}$ kg m^2. The computed torque characteristics (root-mean-square (RMS) and peak torques) and angular velocity requirements (mean and peak velocities) for each assembly are summarized in Table 2. Motor selection was based on the following criteria: (1) stall and peak torque equal to or greater than computed RMS and peak torque, respectively; (2) rated and maximum speed equal to or greater than computed average and peak velocity, respectively. Two servo motors PM-FALR5AM8 (Parker-Hannifin Corporation, Cleveland, OH), which are capable of generating a peak torque of 0.48 N m, a stall torque of 0.16 N m, a rated speed of 3000 rpm, and a maximum speed of 5000 rpm, satisfied those requirements and were selected to drive the cone and tissue mount assemblies.

DISCUSSION

In this study, a novel bioreactor was designed to subject *ex vivo* four cardiovascular tissue specimens to time-varying WSS magnitude and directionality. The device was based on a modified cone-and-plate viscometer in which WSS magnitude was controlled by the cone rotation and WSS directionality was achieved by the rotation of the tissue mounts. While cone-and-plate bioreactors have been used to subject cells and tissue to pulsatile or oscillatory WSS along the circumferential direction, the key innovation brought by this new device is its ability to generate a desired WSS magnitude in a particular direction at each instant of time.

CFD modeling combined with an iterative optimization procedure was used to determine the operating conditions enabling the *in vitro* replication of the native pulsatile and multidirectional WSS environment present on the convexity of the proximal human ascending aorta. Although this WSS environment is specific to this anatomic location, its magnitude and angular temporal characteristics are typical of the WSS experienced by the vascular endothelium. Therefore, it is expected that the strategy implemented in this study for the determination of suitable operating conditions could be applied to the replication of other clinically relevant WSS environments.

Starting with operating conditions directly derived from fluid mechanics theory, only two optimization iterations were necessary to generate the desired WSS magnitude and angle signals on the surface of the tissue specimens. Using those conditions, the stress characteristics predicted on the surface of the tissue specimens closely mimicked the temporal variations of the native magnitude and angle waveforms. It is important to note, however, that the CFD model operated under idealized conditions by neglecting the sutures used to maintain the tissue specimens in position on their mounts. These sutures may generate local flow perturbations and a boundary layer, which could affect the local WSS applied to the tissue. However, the modeling of those sutures in our previous bioreactor design demonstrated their weak impact on the local WSS (correlation coefficient of 0.999 between predicted WSS with and without sutures).[1] In addition, while the level of grid refinement considered in this study was shown to lead to mesh-independent results, a different mesh sensitivity analysis should be performed if a different WSS environment was considered. It is expected that a lower degree of mesh refinement would be required for the replication of a less harsh WSS environment in terms of magnitude, angular range, and temporal gradients. However, this will have to be verified on a case-by-case basis, given the strong connection between the model performance, the mesh characteristics and rotational characteristics of the cone and tissue mounts.

An important consideration is the practicality of the new device relative to other setups. The total cost of fabrication including parts, materials, driving components, and machining is estimated at $6000, which is substantial as compared to less costly setups (e.g., multi-well plates placed on orbital shakers) achieving qualitatively similar periodic variations in WSS magnitude and directionality. However, the key function of our device is to recapitulate the exact changes in WSS directionality experienced by the cardiovascular endothelium *in vivo*. This ability is critical to subject tissue specimens to native physiologic and pathologic WSS environments, and isolate the possible role played by stress abnormalities in cardiovascular disease. Although orbital shakers can effectively subject cells/tissue to time-varying WSS directionality, they do not have the ability to provide control over WSS direction and magnitude simultaneously, and approximate only crudely the *in vivo* environment. Clearly, not all mechanobiological applications require such a fine control over the WSS environment, but those unique capabilities justify the higher cost and level of sophistication of the proposed device.

Many cardiovascular conditions have been associated with hemodynamic abnormalities. For example, valvular abnormalities such as the bicuspid aortic valve

have been shown to increase flow helicity in the ascending aorta, subjecting in turn the aortic endothelium to WSS overloads and increased multidirectionality,[32] which could explain the high prevalence of aortic dilation in those patients. Similarly, aneurysms and atherosclerosis result in anatomical changes in the vasculature, which tend to promote blood flow three-dimensionality and WSS multidirectionality.[21,22,26,36,49] While the etiology of those disorders is still under investigation, there is a growing body of evidence pointing to the key role played by WSS abnormalities in cardiovascular pathogenesis.[2] For example, cone-and-plate devices have been used to link supra-physiologic WSS and abnormal WSS oscillation to early calcification in the context of both the normal tricuspid and abnormal bicuspid aortic valve.[23,39,41,43,44] Similar devices have also been employed to demonstrate the susceptibility of bicuspid aortic valve WSS abnormalities in the aortic wall convexity to trigger focally aortic medial remodeling and degeneration, an early event of dilation.[1,4] However, to date, the effects of WSS directional abnormalities on endothelial biology have not been elucidated. The availability of a device capable of subjecting tissue to desired WSS magnitude and directionality, such as that described in this paper, could be instrumental to a more complete characterization of the role played by hemodynamic stresses in disease initiation and progression.

While this study provides a design solution and mechanical validation of the bioreactor, a biological validation will be necessary prior to the device implementation toward future mechanobiological studies. Experiments with aortic tissue subjected to their native WSS environment will be carried out to verify that the bioreactor maintains sterility, tissue integrity and endothelial function, without promoting cellular apoptosis or changing gross tissue structure. Given the dimensional and operational similarities between this device and our previously validated cone-and-plate bioreactors,[40,42] the proposed design is expected to maintain the structural integrity and viability of tissue specimens for up to 72 h, a duration sufficient for shear-sensitive responses to become evident in cardiovascular tissue.[1,3,23,39,41,43,44]

ACKNOWLEDGMENTS

This work was partially funded by the American Heart Association (Grant-in-Aid 17GRNT33350028), the National Science Foundation (CAREER award 1550144), and the Department of Mechanical and Materials Engineering at Wright State University.

DISCLOSURE

The authors declare that the research was conducted in the absence of any commercial or financial relationships that could be construed as a potential conflict of interest.

REFERENCES

[1]Atkins, S., K. Cao, N. M. Rajamannan, and P. Sucosky. Bicuspid aortic valve hemodynamics induces abnormal medial remodeling in the convexity of porcine ascending aortas. *Biomech. Model. Mechanobiol.* 13:1209–1225, 2014.
[2]Atkins, S. K., A. McNally, and P. Sucosky. Mechanobiology in cardiovascular disease management: potential strategies and current needs. *Front. Bioeng. Biotechnol.* 4:79, 2016.
[3]Atkins, S. K., A. Moore, and P. Sucosky. Bicuspid aortic valve hemodynamics does not promote remodeling in porcine aortic wall concavity. *World J. Cardiol.* 8:89–97, 2016.
[4]Atkins, S. K., and P. Sucosky. The etiology of bicuspid aortic valve disease: focus on hemodynamics. *World J. Cardiol.* 12:1227–1233, 2014.
[5]Bissell, M. M., A. T. Hess, L. Biasiolli, S. J. Glaze, M. Loudon, A. Pitcher, A. Davis, B. Prendergast, M. Markl, A. J. Barker, S. Neubauer, G. Saul, and S. G. Myerson. Aortic dilation in bicuspid aortic valve disease: flow pattern is a major contributor and differs with valve fusion type. *Circ. Cardiovasc. Imaging* 6:499–507, 2013.
[6]Buschmann, M. H., P. Dieterich, N. A. Adams, and H.-J. Schnittler. Analysis of flow in cone-and-plate apparatus with respect to spatial and temporal effects on endothelial cells. *Biotechnol. Bioeng.* 89:493–502, 2005.
[7]Cao, K., S. K. Atkins, A. McNally, J. Liu, and P. Sucosky. Simulations of morphotype-dependent hemodynamics in non-dilated bicuspid aortic valve aortas. *J. Biomech.* 50:63–70, 2017.
[8]Cao, K., and P. Sucosky. Effect of bicuspid aortic valve cusp fusion on aorta wall shear stress: preliminary computational assessment and implication for aortic dilation. *World J. Cardiovasc. Dis.* 5:129–140, 2015.
[9]Cao, K., and P. Sucosky. Computational comparison of regional stress and deformation characteristics in tricuspid and bicuspid aortic valve leaflets. *Int. J. Numer. Method. Biomed. Eng.* 33:e02798, 2017.
[10]Caro, C. G., T. J. Pedley, R. C. Schroter, and W. A. Seed. The Mechanics of the Circulation. Oxford: Oxford University Press, 1978.
[11]Cecchi, E., C. Giglioli, S. Valente, C. Lazzeri, G. F. Gensini, R. Abbate, and L. Mannini. Role of hemodynamic shear stress in cardiovascular disease. *Atherosclerosis* 214:249–256, 2011.
[12]Chakraborty, A., S. Chakraborty, V. R. Jala, B. Haribabu, M. K. Sharp, and R. E. Berson. Effects of biaxial oscillatory shear stress on endothelial cell proliferation and morphology. *Biotechnol. Bioeng.* 109:695–707, 2012.
[13]Chien, S. Mechanotransduction and endothelial cell homeostasis: the wisdom of the cell. *Am. J. Physiol. Heart Circ. Physiol.* 292:H1209–H1224, 2007.

[14]Chung, C. A., M. R. Tzou, and R. W. Ho. Oscillatory flow in a cone-and-plate bioreactor. *J. Biomech. Eng.* 127:601–610, 2005.
[15]Dai, G., S. Natarajan, Y. Zhang, S. Vaughn, B. R. Blackman, R. D. Kamm, G. Garcia-Cardena, and M. A. Gimbrone, Jr. Distinct endothelial phenotypes evoked by arterial waveforms derived from atherosclerosis-susceptible and -resistant regions of human vasculature. *Proc. Natl. Acad. Sci.* 101:14871–14876, 2004.
[16]Davies, P. F. Hemodynamic shear stress and the endothelium in cardiovascular pathophysiology. *Nat. Clin. Pract. Cardiovasc. Med.* 6:16–26, 2009.
[17]Dewey, Jr, C. F., S. R. Bussolari, M. A. Gimbrone, and P. F. Davies. The dynamic response of vascular endothelial cells to fluid shear stress. *J. Biomech. Eng.* 103:177–185, 1981.
[18]Dolan, J. M., H. Meng, S. Singh, R. A. Paluch, and J. Kolega. High fluid shear stress and spatial shear stress gradients affect endothelial proliferation, survival, and alignment. *Ann. Biomed. Eng.* 35:1252–1260, 2011.
[19]Fernández Esmerats, J., J. Heath, and H. Jo. Shear-sensitive genes in aortic valve endothelium. *Antioxid. Redox Signal.* 25:401–414, 2016.
[20]Fewell, M. E., and J. D. Hellums. The secondary flow of Newtonian fluids in cone-and-plate viscometers. *Trans. Soc. Rheol.* 21:535–565, 1977.
[21]Gonzalez, C. F., Y. I. Cho, H. V. Ortega, and J. Moret. Intracranial aneurysms: flow analysis of their origin and progression. *Am. J. Neuroradiol.* 13:181–188, 1992.
[22]Harloff, A., A. Nußbaumer, S. Bauer, A. F. Stalder, A. Frydrychowicz, C. Weiller, J. Hennig, and M. Markl. In vivo assessment of wall shear stress in the atherosclerotic aorta using flow-sensitive 4D MRI. *Magn. Reson. Med.* 63:1529–1536, 2010.
[23]Hoehn, D., L. Sun, and P. Sucosky. Role of pathologic shear stress alterations in aortic valve endothelial activation. *Cardiovasc. Eng. Technol.* 1:165–178, 2010.
[24]Hope, T. A., M. Markl, L. Wigström, M. T. Alley, D. C. Miller, and R. J. Herfkens. Comparison of flow patterns in ascending aortic aneurysms and volunteers using four-dimensional magnetic resonance velocity mapping. *J. Magn. Reson. Imaging* 26:1471–1479, 2007.
[25]Huang, T.-C., C.-K. Chang, C.-H. Liao, and Y.-J. Ho. Quantification of blood flow in internal cerebral artery by optical flow method on digital subtraction angiography in comparison with time-of-flight magnetic resonance angiography. *PLoS ONE* 8:e54678, 2013.
[26]Humphrey, J. D. D., and C. A. A. Taylor. Intracranial and abdominal aortic aneurysms: similarities, differences, and need for a new class of computational models. *Annu. Rev. Biomed. Eng.* 10:221–246, 2008.
[27]Kilner, P. J., G. Z. Yang, R. H. Mohiaddin, D. N. Firmin, and D. B. Longmore. Helical and retrograde secondary flow patterns in the aortic arch studied by three-directional magnetic resonance velocity mapping. *Circulation* 88:2235–2247, 1993.
[28]Kilner, P. J., G. Z. Yang, A. J. Wilkes, R. H. Mohiaddin, D. N. Firmin, and M. H. Yacoub. Asymmetric redirection of flow through the heart. *Nature* 404:759–761, 2000.
[29]Lehoux, S., Y. Castier, and A. Tedgui. Molecular mechanisms of the vascular responses to haemodynamic forces. *J. Intern. Med.* 259:381–392, 2006.
[30]Lehoux, S., and A. Tedgui. Cellular mechanics and gene expression in blood vessels. *J. Biomech.* 36:631–643, 2003.
[31]Levesque, M. J., E. A. Sprague, C. J. Schwartz, and R. M. Nerem. The influence of shear stress on cultured vascular endothelial cells: the stress response of an anchorage dependent mammalian cell. *Biotechnol. Prog.* 5:1, 1989.
[32]Liu, J., J. A. Shar, and P. Sucosky. Wall shear stress directional abnormalities in BAV aortas: toward a new hemodynamic predictor of aortopathy? *Front. Physiol.* 9:993, 2018.
[33]McNally, A., A. Madan, and P. Sucosky. Morphotype-dependent flow characteristics in bicuspid aortic valve ascending aortas: a benchtop particle image velocimetry study. *Front. Physiol.* 8:44, 2017.
[34]Mooney M, Ewart RH. The conicylindrical viscometer. Physics 5:350–354, 350, 1934.
[35]Nerem, R. M. Hemodynamics and the vascular endothelium. *ASME J. Biomech. Eng.* 115:510, 1993.
[36]Peiffer, V., S. J. Sherwin, and P. D. Weinberg. Computation in the rabbit aorta of a new metric—the transverse wall shear stress—to quantify the multidirectional character of disturbed blood flow. *J. Biomech.* 46:2651–2658, 2013.
[37]Pelech, I., and A. H. Shapiro. Flexible disk rotating on a gas film next to a wall. *J. Appl. Mech.* 31:577–584, 1964.
[38]Sdougos, H. P., S. R. Bussolari, and C. F. Dewey. Secondary flow and turbulence in a cone-and-plate device. *J. Fluid Mech.* 138:379–404, 1984.
[39]Sucosky, P., K. Balachandran, A. Elhammali, H. Jo, and A. P. Yoganathan. Altered shear stress stimulates upregulation of endothelial VCAM-1 and ICAM-1 in a BMP-4- and TGF-β1-dependent pathway. *Arterioscler. Thromb. Vasc. Biol.* 29:254–260, 2009.
[40]Sucosky, P., M. Padala, A. Elhammali, K. Balachandran, H. Jo, and A. P. Yoganathan. Design of an ex vivo culture system to investigate the effects of shear stress on cardiovascular tissue. *J. Biomech. Eng.* 130:35001–35008, 2008.
[41]Sun, L., S. Chandra, and P. Sucosky. Ex vivo evidence for the contribution of hemodynamic shear stress abnormalities to the early pathogenesis of calcific bicuspid aortic valve disease. *PLoS ONE* 7:e48843, 2012.
[42]Sun, L., N. M. Rajamannan, and P. Sucosky. Design and validation of a novel bioreactor to subject aortic valve leaflets to side-specific shear stress. *Ann. Biomed. Eng.* 39:2174–2185, 2011.
[43]Sun, L., N. M. Rajamannan, and P. Sucosky. Defining the role of fluid shear stress in the expression of early signaling markers for calcific aortic valve disease. *PLoS ONE* 8:e84433, 2013.
[44]Sun, L., and P. Sucosky. Bone morphogenetic protein-4 and transforming growth factor-beta1 mechanisms in acute valvular response to supra-physiologic hemodynamic stresses. *World J. Cardiol.* 7:331–343, 2015.
[45]Suo, J., J. N. Oshinski, and D. P. Giddens. Blood flow patterns in the proximal human coronary arteries: relationship to atherosclerotic plaque occurrence. *Mol. Cell. Biomech.* 5:9–18, 2008.
[46]Vincent, P. E., A. M. Plata, A. A. E. Hunt, P. D. Weinberg, and S. J. Sherwin. Blood flow in the rabbit aortic arch and descending thoracic aorta. *J. R. Soc. Interface* 8:1708–1719, 2011.
[47]Wang, C., B. M. Baker, C. S. Chen, and M. A. Schwartz. Endothelial cell sensing of flow direction. *Arterioscler. Thromb. Vasc. Biol.* 33:2130–2136, 2013.
[48]Wang, C., H. Lu, and M. A. Schwartz. A novel in vitro flow system for changing flow direction on endothelial cells. *J. Biomech.* 45:1212–1218, 2012.

[49]Yang, Z., H. Yu, G. P. Huang, R. Schwieterman, and B. Ludwig. Computational fluid dynamics simulation of intracranial aneurysms—comparing size and shape. *J. Coast. Life Med.* 3:245–252, 2015.